On the application of variational mechanics in modeling the flow around a cylinder in ground effect

Hever Jonathan Zelaya Solano

Dissertation submitted to the Faculty of the
Virginia Polytechnic Institute and State University
in partial fulfillment of the requirements for the degree of

Master of Science
in
Engineering Mechanics

Mark A. Stremler, Chair
John Domann
Jake Socha

September 12, 2024
Blacksburg, Virginia

Keywords: Potential flow theory, Variational Mechanics, Complex Analysis, Ground Effect, Reduced-order Modeling

On the application of variational mechanics in modeling the flow around a cylinder in ground effect

Hever Jonathan Zelaya Solano

(ABSTRACT)

For high Reynolds number flow over a cylinder near a flat moving surface, a potential flow model can be used to represent flow over the leading edge. However, the potential flow solution requires knowledge of the circulation around the cylinder. This circulation value can be found with an auxiliary condition using energy methods. Two choices for this variational condition exist at present. Gol'dshtik & Khanin (1978) postulated an ad-hoc variational approach that looks only at the velocity on the cylinder boundary. The other approach is guided by the novel work of Gonzalez & Taha (2022), an extension of Gauss' principle that considers the entire velocity field. The first approach was calculated by Petrov & Maklakov (2022), whereas the second approach has not yet been applied to a cylinder in ground effect. These two models are applied to modeling a cylinder in 'ground effect', and the predictions of these two models are compared with a computational fluid dynamics (CFD) simulation by considering the pressure distribution and forces on the cylinder as a function of the cylinder's proximity to the wall. For gap-to-radius ratios approximately between 1 and 6, it is demonstrated that Gauss' principle provides an acceptable auxiliary condition that gives an accurate potential flow representation of the leading-edge flow. The model is also able to calculate the lift coefficient given an approximation of the trailing-edge pressure distribution based on experiment.

On the application of variational mechanics in modeling the flow around a cylinder in ground effect

Hever Jonathan Zelaya Solano

(GENERAL AUDIENCE ABSTRACT)

In this work, the validity of a new reduced-order model that calculates the lift of a cylinder at varying levels of proximity to a flat ground is investigated. The reduced-order model is tested against computational fluid dynamics simulation results from the literature. The derivation of the reduced-order model is analyzed and compared to other similar derivations. It is shown that the investigated reduced-order model is accurate in calculating the lift when the cylinder is approximately one to six radius lengths away from the wall or farther. This makes this model an improved reduced-order model for estimating the lift of a cylinder in ground effect.

Dedication

To my dad, whose decision to leave his homeland has given me boundless opportunities.

To my mother, for her unwavering encouragement and endless compassion.

To my sister, for we are cut from the same cloth; her presence is woven into all I achieve.

And to my uncle Raul, whose memory inspires me to work hard and cherish every endeavor.

Acknowledgments

This work is just one manifestation of the immense support I've received from numerous individuals, who have shaped my character and contributed to my success.

First and foremost, my deepest thanks to my supervisor, Dr. Mark Stremler, for his enthusiasm for this project, unwavering support, encouragement, and patience.

A special thanks to Renee Cloyd for her care and administrative support during my moments of confusion and anxiety about the future. She has been a constant reminder of God's steadfastness and love.

To my family, you deserve more thanks than I can ever give. Your strength and inspiration during my visits home, along with your constant calls and texts, remind me of my worth and vision for life.

I give my utmost thanks to two communities that have sustained me personally and professionally here at Virginia Tech.

The first is the OG group consisting of Nahid, Danielle, Yalda, Zahra, Saim, Mubashar, and Yogesh.

The second is the faith community of Blacksburg Christian Fellowship Church, Jay Lester, Andrew Koser, Victor Lopez, and Josiah Gilbert.

Finally, all that I do is only possible because of the life and freedom that Jesus Christ has offered me. May all my pursuits and accomplishments be done to conform to His Image.

Contents

List of Figures

Chapter 1

Introduction

The problem of a steady incompressible fluid in uniform flow past a circular cylinder is a classical fluid mechanics scenario with both fundamental and practical significance. Understanding this phenomenon is crucial in designing chimney stacks, long-span bridges, tall buildings, towers, heat exchangers, cables, etc., in order to reduce flow forces and induced vibrations that could lead to structural damage. For flow past a circular cylinder, the principal governing parameter is the Reynolds number Re ($= \rho U D/\mu$), which is defined based on the free stream velocity U, diameter of the cylinder D, density of the fluid ρ, and the dynamic viscosity μ. As the value of Re increases, several flow regimes have been observed, such as the onset of vortex shedding, transition to chaos, and successive transitions to turbulence in the wake, the separating shear layer, and the boundary layer [3, 4].

In addition to this classic fluid phenomenon, another common scenario is to place a circular cylinder close to a plane boundary (e.g., ground or seabed), for which the flow is governed not only by Re but also by features of the plane boundary. The flow in this setup may then be affected by [1]

1. the near-wall effect, which is governed by the height-to-radius ratio $h = H/R$,
2. the boundary layer effect, which is governed by the boundary layer thickness δ/R,
3. boundary-layer-induced shear flow (rather than uniform approaching flow) incident on the cylinder (for the case $\delta > R$), and

4. boundary-layer-induced turbulence (rather than steady uniform approaching flow) around the cylinder.

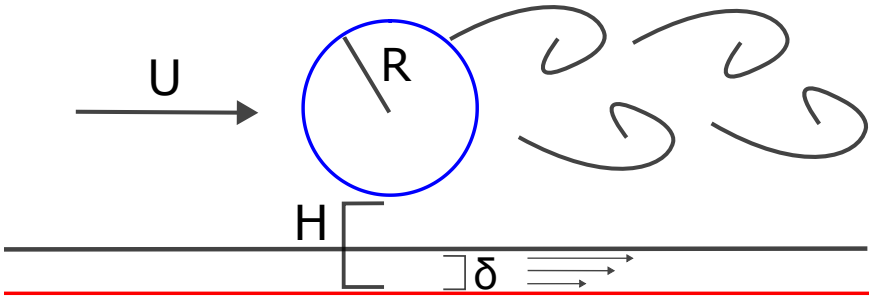

Figure 1.1: Cylinder in ground effect. U is the background flow rate, δ is the boundary layer thickness, H is the gap distance between the cylinder and the ground, and R is the radius of the cylinder. The figure illustrates the vortex shedding occurring behind the cylinder as well as the shear flow generated at the boundary within the boundary layer.

Figure 1.1 illustrates the various parameters that influence the flow for a cylinder near a plane boundary. This flow setup has been studied extensively in the literature using both physical experiments [2, 5, 6, 7], and computational simulations [8, 9, 10, 11]. Much attention has been given to this phenomenon due to its seeming simplicity, its application to offshore pipelines near the seabed, and the potential of extending this understanding of a cylinder in ground effect to more complicated shapes like an airfoil. Because a cylinder in ground effect has a large parameter space (Re, h, δ/R, shear rate, etc.), previous studies generally have focused on the effect of one or two parameters over certain regions of the parameter space. These previous studies show that h is a crucial parameter that governs the flow characteristics and hydrodynamic forces on the cylinder. Although it is observed that the lift coefficient trends with the variation of h [6], understanding this parameter's relation to the others, e.g., δ/R and shear rate, is not clearly understood. Previous studies suggest that differing boundary conditions, such as a moving or stationary ground, provide different critical gap-to-radius values at which the suppression of the alternate vortex shedding is halted [5, 12].

Further studies [11, 13, 14, 15] have considered flow past a circular cylinder in proximity to a plane boundary that moves at a velocity equal to the free stream velocity. As illustrated in figure 1.2, using a moving wall eliminates the streamwise evolution of the boundary layer (and the associated parameters, shear rate, etc.), allowing for a more insightful, focused examination of the near-wall effect.

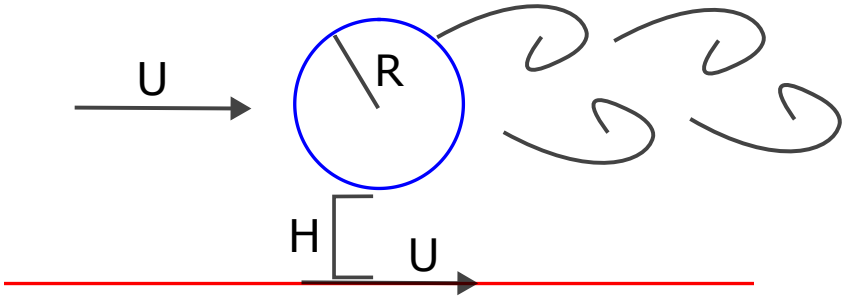

Figure 1.2: Cylinder in proximity to a moving ground. U is the background flow rate, H is the gap distance between the cylinder and the ground, and R is the radius of the cylinder. The moving ground removes the wall-bounded boundary layer and the shear flow generated by this boundary. Compare to figure 1.1

.

Characterizing wake dynamics for flow past a cylinder near a moving ground has warranted much investigation; however, a proper understanding of the interplay between Re (dynamical considerations) and h (geometric considerations) is still unclear. In the literature, studies have been either physical [2, 12, 16], or computational [1, 17, 18] simulations, whereas there is only one proposed analytical model for this system [18].

Starting with the open-form analytical solution for a cylinder near a plane boundary proposed by Baddoo et al. [19], all that is required to completely solve the velocity field is a closure condition. The closure condition for this model is the value of the circulation around the cylinder. For modeling an airfoil using potential flow theory, the auxiliary condition takes the form of the Kutta condition, which asserts that the circulation imposed on the boundary

is such that the velocity at the trailing edge is finite [20]. This approach works for airfoils with sharp-trailing edges. Also, ad-hoc generalizations have been proposed for blunt-trailing edges [21, 22, 23, 24]; however, for a cylinder, **any** value of the circulation gives a finite velocity and is a permissible solution. In this thesis, two proposed auxiliary conditions are investigated that are based on variational (energy) principles [25, 26]. By beginning with a general statement of some minimized quantity in a system, a variational principle approach is one that ensures the solution maintains the minimax of said quantity. The two variational approaches investigated are

1. **Gol'dshtik's Postulate (GP):** Nature wants to minimize the maximum velocity on the contour of the body, seeking to conserve the linear momentum on the boundary, proposed by Gol'dshtik in 1978 [25].

2. **Principle of Minimum Pressure Gradient (PMPG):** Nature wants to minimize the overall curvature of the system, which for an ideal fluid reduces to the conservation of the pressure gradient over the whole flow field (Gonzalez & Taha, 2022) [26]. This recently proposed principle is established by a theoretically rigorous derivation that could be revolutionary in its application of variational mechanics in fluids. However, the legitimacy of the theory is still in question, and a second objective of this thesis is to investigate its versatility.

The prior model was built by Petrov & Maklakov [18] using Gol'dshtik's postulate as the auxiliary condition to the potential flow formulation for a cylinder in ground effect. The authors calculate the pressure coefficient values around the contour of the cylinder but do not compare model results with experimental or CFD data on the lift coefficient or the leading-edge stagnation point. At the time, the principle of minimum pressure gradient had not been published, leaving GP as the only auxiliary condition.

In this thesis, a new reduced-order model is constructed by implementing the PMPG auxiliary condition. The model is compared with Petrov's [18] solution (denoted as GP method) by looking at the lift coefficient and leading-edge stagnation point values for a range of gap-to-radius distances. Since Petrov & Maklakov [18] do not provide information about the lift coefficient or leading-edge stagnation point, this work provides the calculations for those as well. What this work aims to do is twofold:

1. investigate the usefulness of a potential flow model for a cylinder in ground effect,
2. use the reduced-order model to gain insight into the physics of a cylinder in ground effect.

The investigation of a potential model's usefulness and physical insight for this problem is accomplished in two parts. First, both variational closure conditions are investigated assuming the whole flow field is appropriately modeled by potential flow. Second, improvements to the potential flow model are considered by using CFD data to approximate the trailing-edge dynamics while continuing to approximate the leading-edge as a potential flow. Petrov [18] has done work to improve his model using a different approach; however, his extension isn't utilized due to its numerical complexity and lack of data provided by him. More discussion on this in section 5.2.

For this work, the computational fluid dynamics (CFD) simulations by Jiang et al. [1] were used as a reference for information about the mean lift coefficient. The reduced-order models were also compared with the trailing-edge flow separation angles and leading-edge stagnation angle since this data was also provided by the CFD. Figure 1.3 and 1.4 show the lift coefficient and flow separation points from fifty high-fidelity three-dimensional direct numerical simulations performed over a parameter space of Reynolds numbers of 300, 400, 600, 800, and 1000 and h values of 0.4, 0.6, 0.8, 1.0, 1.2, 1.6, 2.0, 3.0, and 6.0. [1]

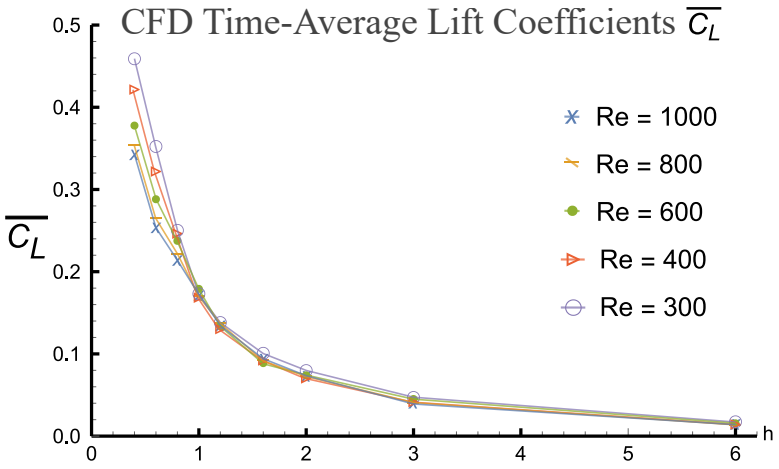

Figure 1.3: Time-averaged lift coefficient from Jiang *et al.*[1] CFD simulations at $Re = 300$, 400, 600, 800, and 1000. The lift coefficients at varying Reynolds number seem to converge as h increases.

In this document, two general potential flow solutions are investigated for their accuracy in calculating the lift coefficient of a cylinder in ground effect. A post-processed model is also considered that uses a modified trailing-edge pressure distribution informed by experimental data. The overall aim of this work is to contribute to the development of a theoretical model and thereby gain insight into the physics of a cylinder in ground effect.

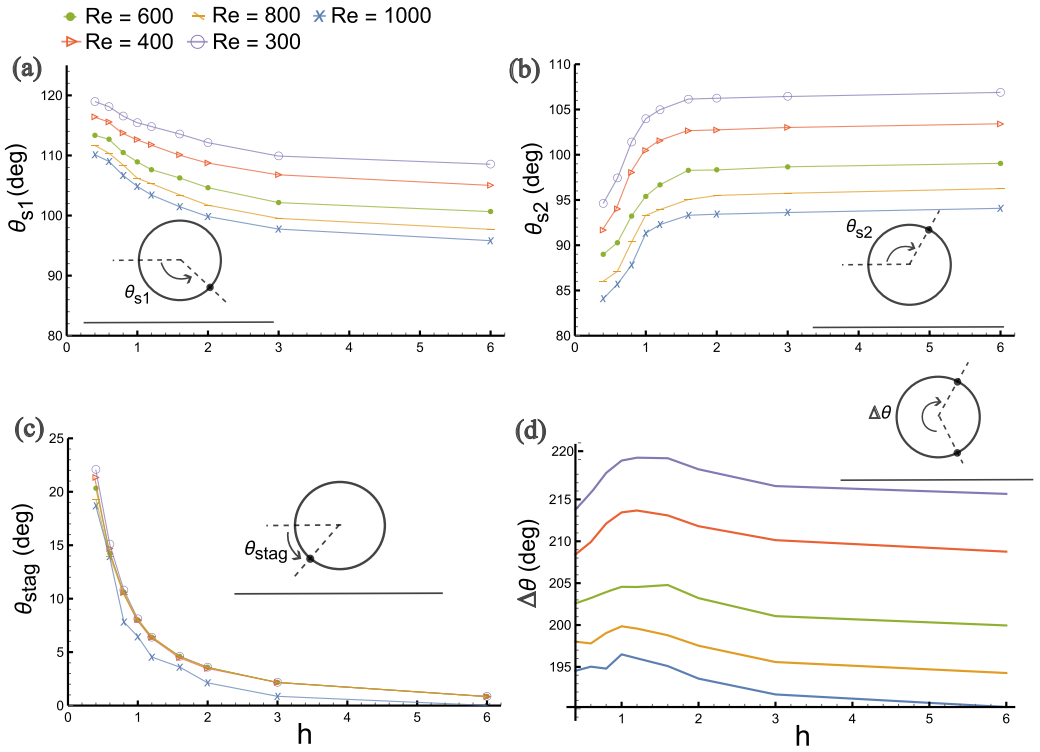

Figure 1.4: CFD simulation separation, stagnation, and span angle values for $Re = 300$, 400, 600, 800, and 1000. *a)* lower leading-edge separation angle, *b)* upper leading-edge separation angle, *c)* leading-edge stagnation point, and d) the leading-edge angle span using *a)* and *b)*.

Chapter 2

A general reduced-order model

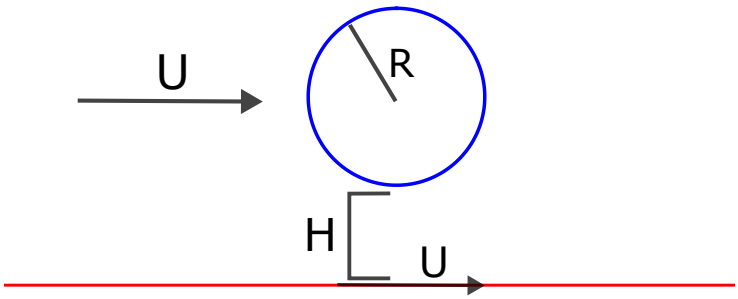

Figure 2.1: Schematic of a cylinder in proximity to a moving ground. The vorticity is not explicitly represented in the formulation of the system in this thesis. This work considers a cylinder moving through an inviscid fluid, neglecting the wake structure behind the cylinder.

Figure 2.1 illustrates the system to which the potential model is applied. Unlike figure 1.2, the vorticity is not explicitly represented in the system formulation in this thesis. Defining the fluid velocity vector field as $\vec{u}$, the assumptions for the flow field are 1) the fluid is incompressible ($\nabla \cdot \vec{u} = 0$), 2) the fluid is inviscid (has zero viscosity), 3) the flow is irrotational ($\nabla \times \vec{u} = 0$), 4) the flow is steady ($\partial \vec{u}/\partial t = 0$), 5) the ground is moving at the same speed as the background flow U, and 6) we can reduce the system to a 2-dimensional slice of the true 3-dimensional flow field as illustrated in figure 2.1.

For steady, incompressible, inviscid fluids, the flow dynamics are determined by solving the velocity field, $\vec{u}$, that satisfies the Euler equations

$$\rho \vec{u} \cdot \nabla \vec{u} = -\nabla p, \quad \text{in } \Omega, \tag{2.1}$$

where ρ, p and Ω are the fluid density, pressure, and domain, respectively. The flow must satisfy the no-penetration boundary condition

$$\vec{u} \cdot \vec{n} = 0, \quad \text{on } \partial\Omega, \tag{2.2}$$

where $\partial\Omega$ is the domain boundary and $\vec{n}$ is the normal vector to the boundary.

A general solution to this equation for a cylinder in ground effect can be determined analytically thanks to three elements. First, the 3D flow field can be reduced to a 2D flow problem, which allows the use of complex analysis. Secondly, assuming the flow is irrotational ($\nabla \times \vec{u} = 0$) allows the complex formulation to be a mathematically allowable solution. Thirdly, the development of conformal mapping of more general multiply connected domains for solving fluid problems, such as a cylinder near a wall allows for the construction of an analytical solution [27].

The mathematical solution proposed by Baddoo [19] first requires an appropriate coordinate transformation from a doubly connected annulus to a cylinder over a flat ground, as can be seen in figure 2.2. Secondly, the construction of the correct complex potential inside the annulus is needed.

2.1 Defining the flow field

Considering an ideal fluid with flow velocity $\vec{u}$ in a physical z-plane with $z = x + iy$, the complex potential can be defined as

$$f(z) = \phi(z) + i\psi(z), \tag{2.3}$$

where ϕ and ψ are the velocity potential and streamfunction in the physical z-plane, respectively. The complex velocity, $w = u_x - iu_y$, can be calculated as

$$w(z) = \frac{df}{dz}. \tag{2.4}$$

An introduction to the treatment of fluid flow using complex analysis can be found, for example, in [28].

2.1.1 Conformal mapping

A cylinder in ground effect can be described using conformal mapping. The annular domain (ζ-plane) is mapped to the physical domain (z-plane) as illustrated in figure 2.2. The annulus is defined as two concentric circles, where the outer circle is a unit disc (denoted C_1) and the inner circle (denoted C_0) has radius q. The appropriate mapping function is a standard Möbius map [19]

$$z = g(\zeta) = \frac{1-q^2}{4iq} \times \frac{\zeta+1}{\zeta-1}, \tag{2.5}$$

which maps C_1 to the real axis and C_0 to a circle of unit diameter centered at $i(q+q^{-1})/4$.

The value q is a function of h given by

$$q = (h+1) - \sqrt{(h+1)^{1/2} - 1}. \tag{2.6}$$

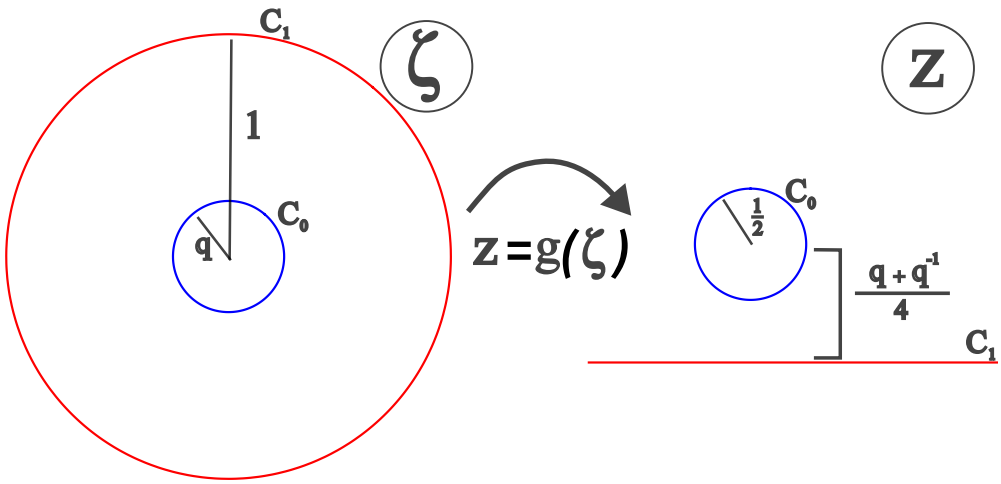

Figure 2.2: Conformal mapping from an annulus (ζ-plane) to a cylinder over a flat ground (z-plane) using equation 2.5. The outer circle C_1 of unit radius in the ζ-plane maps to the infinitely long flat ground in the z-plane, and the inner circle C_2 of radius q in the ζ-plane maps to the cylinder of radius $\frac{1}{2}$ centered at $\frac{q+q^{-1}}{4}$in the z-plane.

2.1.2 The complex velocity

With the conformal mapping from the annular domain to the physical domain, it is sufficient to calculate the complex potential in the annular domain and then map this solution to the physical domain. The complex potential in the ζ-plane is expressed as $F(\zeta) = f(z) = f(g(\zeta))$.

The appropriate complex potential is achieved by using one of the special transcendental functions, the 'Schottky-Klein prime functions' [27]. The function is expressible as the infinite product

$$P(\zeta) = (1-\zeta)\prod_{k=1}^{\infty}(1-q^{2k}\zeta)(1-q^{2k}\zeta^{-1}), \tag{2.7}$$

for $0 < q < 1$. The dependence on q is suppressed here for notational convenience. A full discourse on this special function can be found in the works of Crowdy [27]. This special

function is typically used to solve fluid dynamics problems in multiply connected domains such as stacked airfoils [27]. Given that $P(\zeta)$ is analytic in the annulus $q < |\zeta| < q^{-1}$, except for a simple zero at $\zeta = 1$, it can be used to model a cylinder near a wall.

The complex potential of a cylinder in ground effect is constructed as a superposition of the background uniform flow and a circulatory flow around the cylinder. The complex potential for the background flow is [19]

$$F_U(\zeta) = U\zeta \frac{1-q^2}{i2q} \frac{P'(\zeta)}{P(\zeta)}. \tag{2.8}$$

The circulatory flow complex potential is

$$F_\Gamma(\zeta) = \frac{\Gamma}{2\pi i} \log \zeta, \tag{2.9}$$

where Γ is the 'induced' circulation on the contour of the cylinder. The complete general complex potential in the ζ-plane is then

$$F(\zeta) = U\zeta \frac{1-q^2}{i2q} \frac{P'(\zeta)}{P(\zeta)} + \frac{\Gamma}{2\pi i} \log \zeta. \tag{2.10}$$

Representative streamlines in the material and spatial domain are shown in figure 2.3.

Applying equation 2.5, the velocity in the spatial domain in ζ-coordinates is

$$W(\zeta) = w(g(\zeta)) = \frac{df(g(\zeta))}{d(g(\zeta)))} = \frac{1}{g'(\zeta)} \frac{dF(\zeta)}{d\zeta} = G(\zeta) \frac{dF(\zeta)}{d\zeta}, \tag{2.11}$$

where $1/g'(\zeta) = G(\zeta)$. The ζ dependence will be dropped for notational convenience. If the function is dependent on something other than ζ, that will be made explicit. The complete

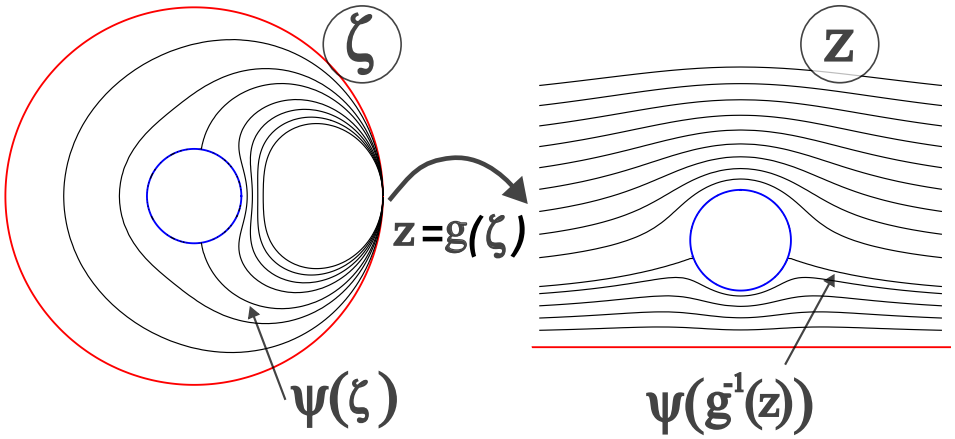

Figure 2.3: Streamlines, Ψ, in the annulus (ζ-plane) and spatial domain (z-plane) are shown by taking the imaginary component of the complex potential given in equation 2.10. Gap-to-radius ratio is 1 and Γ is -1.

velocity field can be expressed as

$$W = UG\frac{1-q^2}{i2q}\left(\frac{P(P'+\zeta P'')-\zeta P'^2}{P^2}\right)+\frac{G\,\Gamma}{2\pi i\zeta}, \tag{2.12}$$

where

$$G = \frac{2iq(\zeta-1)^2}{q^2-1}. \tag{2.13}$$

This expression satisfies the Euler equations for an incompressible, irrotational, inviscid flow for a cylinder in ground effect. The parameters q and U are system dependent. However, the circulation value Γ is unknown, for which infinite choices exist. Baddoo [19] proposes implementing the Kutta condition to calculate the circulation; however, for a cylinder this condition states that the velocity at the trailing-edge is finite. For a cylinder, the velocity will always be finite, and thus the Kutta condition is a poor auxiliary condition in this case.

2.1.3 Bounds of Γ

Although the value of Γ can take on any value and still satisfy the Euler equations, realistic bounds on the circulation value can be determined. As seen in figure 2.4, there are two instances in which the stagnation points take on a single value on the contour. Given that any value Γ outside this range describes a flow with a stagnation point detached from the body, those values are discarded since they do not align with the experimental data. The range of Γ is therefore given by

$$\Gamma_{\min} \leq \Gamma \leq \Gamma_{\max}.$$

The values of the maximum and minimum circulation are calculated by setting the velocity equal to zero on the contour and solving for Γ when ζ is placed on the north and south pole of the cylinder. This procedure gives

$$\begin{aligned}
\Gamma_{\min} &= -U\pi\xi_{\min}(1-q^2)\left(\frac{P(\xi_{\min})(P'(\xi_{\min})+\xi_{\min}P''(\xi_{\min}))-\xi_{\min}P'(\xi_{\min})^2}{P(\xi_{\min})^2}\right) \\
\Gamma_{\max} &= -U\pi\xi_{\max}(1-q^2)\left(\frac{P(\xi_{\max})(P'(\xi_{\max})+\xi_{\max}P''(\xi_{\max}))-\xi_{\max}P'(\xi_{\max})^2}{P(\xi_{\max})^2}\right),
\end{aligned} \tag{2.14}$$

where

$$\begin{aligned}
\xi_{\min} &= \left(\frac{q+q^{-1}}{4}-\frac{1}{2}\right)e^{i\frac{\pi}{2}} \\
\xi_{\max} &= \left(\frac{q+q^{-1}}{4}+\frac{1}{2}\right)e^{i\frac{\pi}{2}}.
\end{aligned} \tag{2.15}$$

The range of circulation values as a function of h can be seen in figure 2.5. The gap between the maximum and minimum circulation decreases drastically from $h \in \{0, 1\}$ and converges to a constant range for $h > 5$. The range of possible circulation values is largest for small h, which highlights the system's sensitivity to circulatory effects when the cylinder is near the wall.

The focus of this work now becomes clear. The potential flow solution for a cylinder in ground

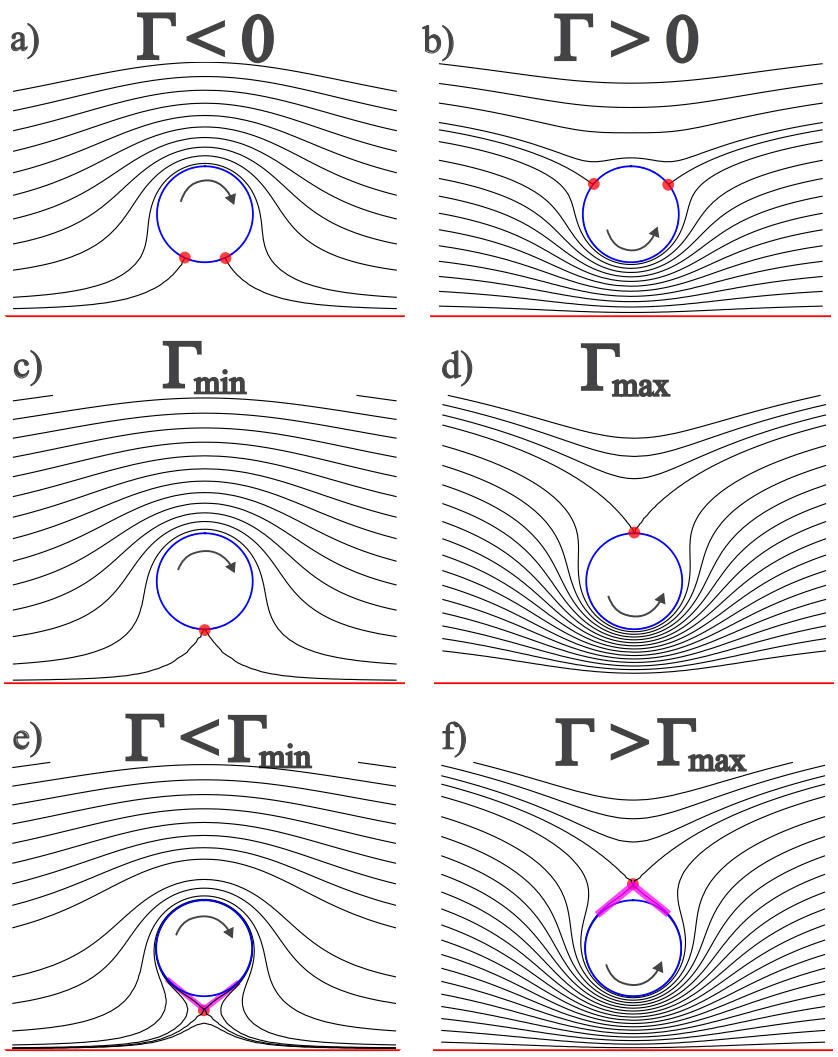

Figure 2.4: The streamlines for varying values of Γ are shown. Panels *a,b)* Illustrate how perturbing the value of Γ influences the location of the stagnation point and the corresponding flow field. Panels *c,d)* Illustrate the maximum and minimum values the circulation can have before having the stagnation point leave the contour of the cylinder. Panels *e,f)* Illustrate what occurs to the bluff body streamline if the circulation exceeds the $\Gamma_{\max}$ and $\Gamma_{\min}$ values, causing the stagnation point to leave the contour of the body.

effect does not uniquely determine the flow field and an auxiliary condition is needed. As mentioned in the introduction of this chapter, two variational approaches will be used as constraint equations to calculate a unique Γ fully solving the flow field. This calculation is done in chapter 3.

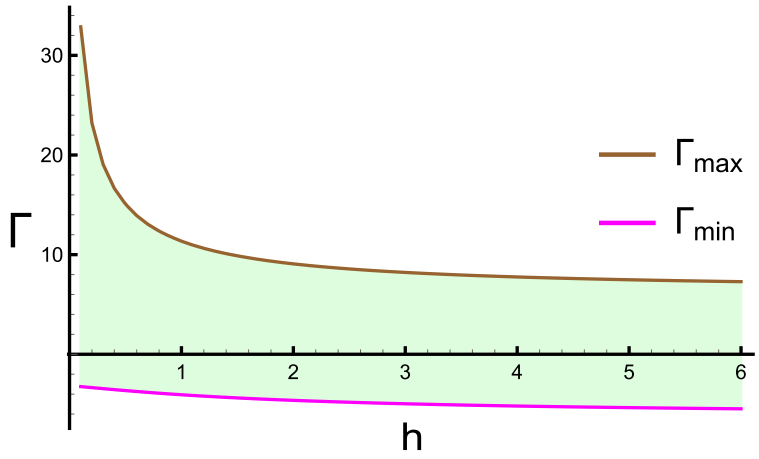

Figure 2.5: Admissible circulation values

2.2 Defining Lift and Pressure Coefficients

Having a complete flow field solution allows for the calculation of important physical quantities such as the lift and drag coefficient. These are calculated by first determining the pressure of the flow.

Pressure coefficient

The pressure coefficient was calculated by using the steady incompressible Bernoulli equation to find the pressure,

$$P = P_0 + \frac{1}{2}\rho(U^2 - |W|^2), \tag{2.16}$$

where P_0 is the reference pressure. The pressure coefficient is defined as

$$C_P = \frac{P - P_0}{\frac{1}{2}\rho U^2} = 1 - \left|\frac{W}{U}\right|^2. \tag{2.17}$$

Lift and Drag Coefficient

The lift coefficient is defined as

$$C_L = \frac{F_L}{\frac{1}{2}\rho U^2 A} \tag{2.18}$$

where F_L is the lift force and A is the cross-sectional area of the cylinder as viewed from the incoming flow. The forces acting on the cylinder are determined by integrating the pressure around the contour. The local force, dF, when decomposed into drag and lift components can be written as

$$dF = dF_D - idF_L = -Pdy - iPdx = -iP(dx - idy). \tag{2.19}$$

Integrating around the contour gives the entire force acting on the cylinder

$$F_D - iF_L = -i \oint_{\partial\Omega} P \, dz^* = -i \oint_{\partial\Omega} ((P_0 + \frac{1}{2}\rho U^2) - \frac{1}{2}\rho |W|^2) \, dz^*. \tag{2.20}$$

where the star, *, represents complex conjugation. A similar derivation to Blasius force theorem is applied here [22]. Since the integral is over a closed contour, the force contribution from $P_0 + \frac{1}{2}\rho U^2$ is zero exactly. Simplifying, the lift coefficient gives

$$C_L = -\frac{1}{A}\mathrm{Im}\left[i \oint_{\partial\Omega} \left|\frac{W}{U}\right|^2 dz^* \right] = -\frac{1}{A}\mathrm{Im}\left[i \oint_{\partial\Omega} \left(\frac{W}{U}\right)^2 dz \right] = -\frac{1}{A}\mathrm{Im}\left[i \oint_{\partial\Omega} (1 - C_p) dz^* \right]. \tag{2.21}$$

Chapter 3

Auxiliary conditions based on variational principles

The general solution for the flow field presented in chapter 2 was found via kinematic considerations. However, the model does not account for dynamical considerations, and consensus on the appropriate auxiliary condition for calculating Γ has not been reached [26].

When solving physics-based problems, approaches to calculate the constraint equations are important. A widely used tool for this approach is variational (analytical) mechanics [29, 30, 31]. The basic idea of this method is to assert that nature (or the system) is trying to optimize some *special* quantity in all space and time. If this is true, then depending on the form of the solution, the unknown parameters or functions take on the necessary value or function that minimize that *special* quantity. The *special* quantity is often called the *Action*. If one is able to determine the *Action*, what is left is an optimization problem to uniquely determine the unknowns. For a cylinder in ground effect, the appropriate question to ask would be 'What is the quantity that an incompressible fluid optimizes for all flow?' Once the *Action*, A, is determined, the free parameter Γ can be solved by applying a derivative and solving for the circulation,

$$\frac{dA(\vec{u}(\vec{x};\Gamma))}{d\Gamma} = 0 \rightarrow \Gamma_{\text{solution}}. \tag{3.1}$$

In the literature, only two variational approaches have been proposed that can be used to model a cylinder in ground effect. The first is Gol'dshtik's postulate proposed in 1977 [18, 25], and the second is the principle of minimum pressure gradient, PMPG, variational principle [26], which has not previously been applied to a model of a cylinder in ground effect.

3.1 Gol'dshtik Postulate

Gol'dshtik's postulate is based on the fact that a cylinder near the ground produces a wake. Gol'dshtik asserts that the circulation value that occurs around a cylinder in ground effect is the one that maximally prevents separation. He states, "*A natural characteristic of this [cylinder in ground effect] phenomenon is the maximum value of the velocity at the contour: the higher it is, the greater is the pressure drop and the more probable is a separation, due to the effect of the viscosity with restoration of pressure. Thus, as a possible alternative for generalization of the postulate concerning the circulation, the minimax variational principle is considered below: with real flow-around, the circulation assumes a value which will minimize the maximum velocity at the contour*" [25]. It is important to note that this variational principle is applied only to the contour of the cylinder and does not take into account any of the flow dynamics happening in the rest of the system.

The *Action* postulated by Gol'dshtik (GP) can be written as

$$A_{\mathrm{GP}}(\Gamma) = \max\left[\left|W(\zeta;\Gamma)\right|\Big|_{\partial\zeta}\right], \tag{3.2}$$

where the magnitude of the velocity in the spatial plane is evaluated all along the contour of the cylinder in terms of the reference frame coordinates, ζ. Once this function is differentiated

with respect to Γ, it becomes a simple optimization problem, given by

$$\frac{d}{d\Gamma}\left(\max\left[|W(\zeta;\Gamma)|\Big|_{\partial\zeta}\right]\right) = 0 \rightarrow \Gamma_{\text{gol}}. \tag{3.3}$$

Calculating $\max\left[|W(\zeta;\Gamma)|\Big|_{\partial\zeta}\right]$ is straightforward. The coordinates in the ζ-plane are polar coordinates $\{r,\theta\}$ where $\partial\zeta = q\ e^{i\theta}$. Evaluating the magnitude of the complex velocity on the contour gives an expression in terms of θ and Γ, $|W(\theta;\Gamma)|\Big|_{\partial\zeta}$. The location of the maximum velocity is where the derivative of the velocity with respect to θ is zero, and the minimization of the maximum velocity is done by taking a derivative of the velocity with respect to Γ. Solving these simultaneously will allow for the calculation of the circulation,

$$\frac{\partial|W_{\partial z}(\theta;\Gamma)|}{\partial\theta} = 0, \quad \frac{\partial|W_{\partial\zeta}(\theta;\Gamma)|}{\partial\Gamma} = 0. \tag{3.4}$$

The derivation is tedious, but Petrov & Maklakov [18] show that the circulation value can be expressed as

$$\Gamma_{\text{GP}} = \frac{1}{2}(\Gamma_{\min} + \Gamma_{\max} + \frac{\Gamma_{\min} - \Gamma_{\max}}{h+1}). \tag{3.5}$$

3.2 The principle of minimum pressure gradient

Gol'dshtik's postulate only considers the contour of the cylinder as the causal factor for the uniqueness of the circulation. We will now direct our attention at a variational principle that takes into account the entire flow field for its constraint formulation.

A recent publication by Taha & Gonzalez [32] provides a theoretically rigorous development for using variational mechanics in fluids. The variational principle asserts that every incom-

pressible flow minimizes the pressure gradient. This principle is built on Gauss' principle of least constraint or least squares. Gauss defines the *Action* [33],

$$S = \int_{\Omega} \frac{1}{2}\rho \, (\vec{a}_{\text{constraint}})^2 \, d\vec{x}, \tag{3.6}$$

as the quantity being minimized. Gauss asserted that nature wants to minimize the constraint forces in a system. For a fluid, Taha & Gonzalez [32] showed that the pressure gradient is the constraint force for every incompressible fluid problem. Therefore, rewriting the *Action* with $\vec{a}_{\text{constraint}} = \nabla p = \vec{u} \cdot \nabla \vec{u}$, gives

$$S = \frac{1}{2}\rho^{-2} \int_{\Omega} (\nabla p(\vec{x}; \Gamma))^2 \, d\vec{x} = \frac{1}{2}\rho^{-2} \int_{\Omega} [\vec{u}(\vec{x}; \Gamma) \cdot \nabla \vec{u}(\vec{x}; \Gamma)]^2 \, d\vec{x}. \tag{3.7}$$

Taha & Gonzalez [26] call this variational approach the *Principle of Minimum Pressure Gradient* or PMPG.

In complex notation the *Action* in this case can be expressed as

$$S = \frac{1}{2}\rho^{-2} \int_{C} |w(z)(\frac{dw(z)^*}{dz})|^2 \, dz = \frac{1}{2}\rho^{-2} \int_{\Omega} |W(G\frac{dW}{d\zeta})^*|^2 \, \frac{d\zeta}{|G|^2}. \tag{3.8}$$

The appropriate coordinate transformation for the differential terms in the integration are shown and derived in appendix A.1.

Rewriting W will allow for a simple analytical expression for Γ. This is done in the following way. First, factor W into the background and circulatory flow components

$$W = UW_U + \Gamma W_\Gamma, \tag{3.9}$$

where

$$W_U = G\frac{1-q^2}{i2q}\left(\frac{P(P'+\zeta P'')-\zeta P'^2}{P^2}\right),$$
$$W_\Gamma = \frac{G}{2\pi i\zeta}, \tag{3.10}$$

are the complex velocities from the background flow and the imposed circulation, respectively. U and Γ are factored for analytical convenience since they are dynamical parameters, whereas all the terms inside W_U and W_Γ are geometric parameters. Substituting equation 3.9 into equation 3.8, the new form of the *Action* becomes

$$S = \frac{1}{2}\rho^{-2}\int_\Omega \Big(U^4|a_U|^2 + \Gamma^4|a_\Gamma|^2 + U^2\Gamma^2(|a_{U\Gamma}|^2 + 2\mathrm{Re}[a_U a_\Gamma^*]) \\ +2U^3\Gamma\mathrm{Re}[a_{U\Gamma}a_U^*] + 2U\Gamma^3\mathrm{Re}[a_{U\Gamma}a_\Gamma^*]\Big)\frac{d\zeta}{|G|^2}, \tag{3.11}$$

where

$$a_U = G^* W_U\left(\frac{\partial W_U}{\partial\zeta}\right)^*,$$
$$a_\Gamma = G^* W_\Gamma\left(\frac{\partial W_\Gamma}{\partial\zeta}\right)^*, \tag{3.12}$$
$$a_{U\Gamma} = G^* W_\Gamma\left(\frac{\partial W_U}{\partial\zeta}\right)^* + G^* W_U\left(\frac{\partial W_\Gamma}{\partial\zeta}\right)^*.$$

This can be further simplified as

$$S = \frac{1}{2}\rho\Big(U^4\alpha + \Gamma^4\beta + U^2\Gamma^2\gamma + U^3\Gamma\kappa + U\Gamma^3\epsilon\Big), \tag{3.13}$$

where

$$\begin{aligned}
\alpha &= \int_\Omega |a_U| \, \frac{d\zeta}{|G|^2}, \\
\beta &= \int_\Omega |a_\Gamma| \, \frac{d\zeta}{|G|^2}, \\
\gamma &= \int_\Omega |a_{U\Gamma}| + 2\mathrm{Re}[a_u a_\Gamma^*] \, \frac{d\zeta}{|G|^2}, \\
\kappa &= \int_\Omega 2\mathrm{Re}[a_{U\Gamma} a_U^*] \, \frac{d\zeta}{|G|^2}, \\
\epsilon &= \int_\Omega 2\mathrm{Re}[a_{U\Gamma} a_\Gamma^*] \, \frac{d\zeta}{|G|^2}.
\end{aligned} \tag{3.14}$$

Differentiating the *Action* and setting it to zero results in the following cubic expression

$$\frac{dS}{d\Gamma} = 0 \quad \rightarrow \quad 4\beta\Gamma^3 + 3\epsilon U\Gamma^2 + 2\gamma U^2\Gamma + U^3\kappa = 0, \tag{3.15}$$

which can be solved once the coefficients of the expression are calculated. Remember that all the parameters are functions of h. It is easier to rewrite the expression in terms of (Γ/U) and solve for a 'relative' circulation value,

$$4\beta(h)(\frac{\Gamma}{U})^3 + 3\epsilon(h)(\frac{\Gamma}{U})^2 + 2\gamma(h)(\frac{\Gamma}{U}) + \kappa(h) = 0. \tag{3.16}$$

With the ability to vary h, which alters the integral values in 3.14, equation 3.16 gives an expression to calculate the circulation as a function of h, $\Gamma_{\mathrm{PMPG}}(h)$.

Chapter 4

Numerical Methods

Wolfram Mathematica was used to compute circulation values using both GP and PMPG. Mathematica's symbolic algebraic library contains Jacobi Theta-functions and Prime functions, which were crucial in computing equations 2.7, 2.8, and 2.15. These were calculated using the numerical integration function *NIntegrate*.

Γ was calculated for h values in the range $0.1 \leq h \leq 10$, at a step size of $\Delta h = 0.1$, with $\rho = 1$, and $U = 1$. A continuous solution for $\Gamma(h)$ was found by linearly interpolating between the explicit h values used to calculate Γ. This interpolation procedure was also used with the simulation data from Jiang et al. [1], which allowed for a continuous comparison between the analytical solution and the simulation results.

Chapter 5

Analytical model results

Figure 5.1 shows the circulation values calculated using both variational methods from 3.5 3.16. Fortunately, both methods are well within the physically-allowed circulation range. Both models predict negative circulation, which will result in a positive lift coefficient. It is expected the PMPG will yield a larger lift force since the increase in circulation relative to the GP values will generate a lower pressure above the cylinder.

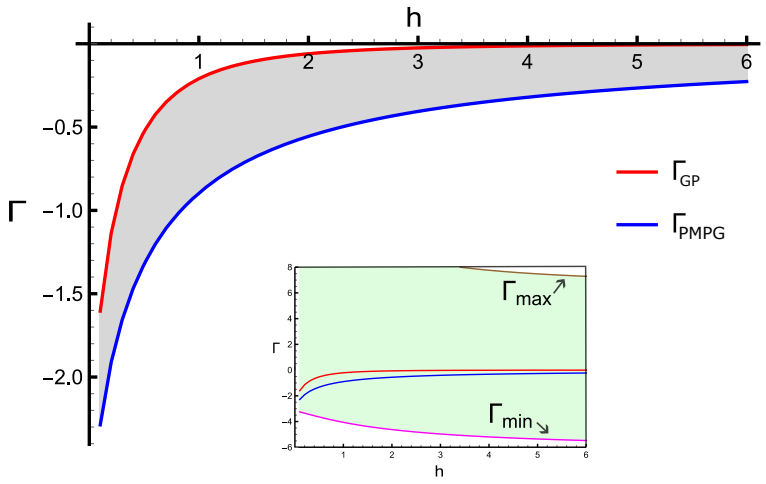

Figure 5.1: GP and PMPG circulation values over the range $h \in \{0.1, 6\}$. The inset panel shows how the variational method circulation values are within the domain of allowable circulation values from figure 2.5.

It is interesting to note the slight difference in the streamlines between the models. Figure 5.2 illustrates the two streamlines at $h = 1$. At first glance, the difference appears small. How significantly does this seemingly small difference in the circulation values impact the

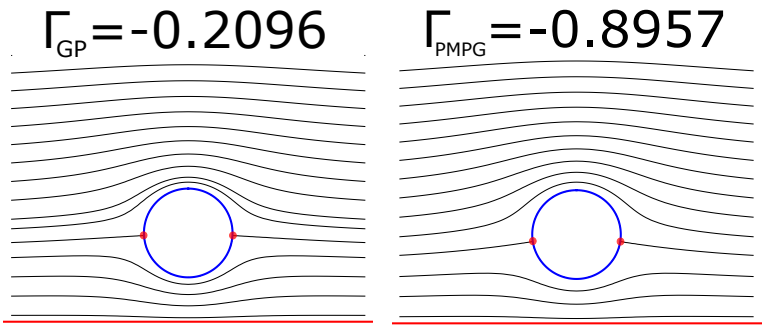

Figure 5.2: Representative streamlines of GP and PMPG at $h = 1$.

lift coefficient of the system?

5.1 Lift coefficient results

The corresponding lift coefficients from each model compared with the CFD simulations from [1] are shown in figure 5.3. It should be emphasized that these models actually (and perhaps amazingly) capture the $C_L(h)$ trend. This agreement is quite remarkable given that the potential flow framework does not take into account turbulence or separation of the flow.

The GP approach produces a lift coefficient well below the CFD simulations [1] for all values of h. In contrast the PMPG approach for $h > 1$ produces a lift coefficient that over-predicts the CFD results. The resultant lift coefficient from the CFD simulations [1], GP, and PMPG all tend to zero; however PMPG approaches zero at rate relative to h about 10^6 slower than both GP and simulation. The PMPG seems to present high sensitivity to the presence of the wall even at large distances. Although in the limit as $h \to \infty$ the lift coefficient is zero using PMPG, the slow rate of change should be further investigated as it may reveal an artifact in either the computation or the variational approach. However, for $h < 1$ the PMPG approach seems to capture the correct order of magnitude of the lift coefficient.

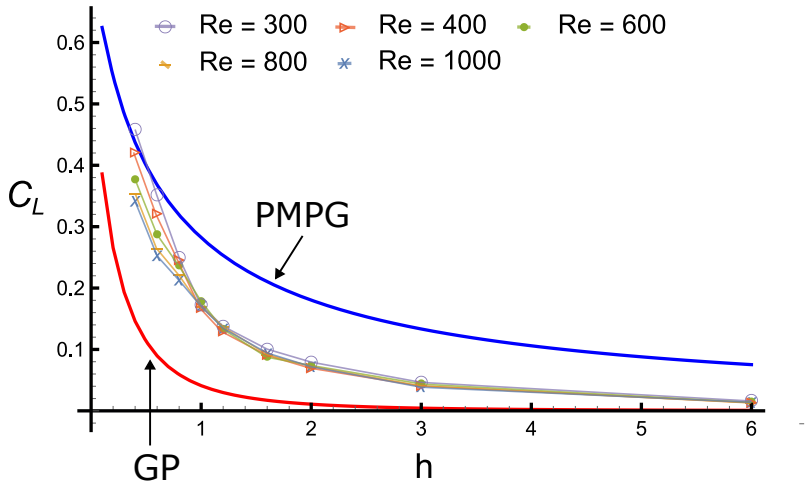

Figure 5.3: Lift coefficient values from the CFD simulations [1], GP, and PMPG model for $h \in \{0.1, 6\}$.

The root-mean-squared-percent-error between the simulation data and the two models was calculated via

$$C_{\mathrm{L,RMS}} = \sqrt{\frac{1}{h_f - h_i} \int_{h_i}^{h_f} \left[\frac{C_{\mathrm{L,th}}(h) - C_{\mathrm{L,sim}}(h)]}{C_{\mathrm{L,sim}}(h)} \right]^2 dh} \times 100\%, \tag{5.1}$$

where h_f and h_i are the initial and final gap-to-radius ratios, h, of the CFD simulations.

Figure 5.4 illustrates the percent error of each method in a box and whisker plot. The box and whisker plot captures the mean, median, and outlier of the percent error along the varying h values. The percent error over the h domain was 88.7% and 198.2% for Gol'dshtik and PMPG method, respectively.

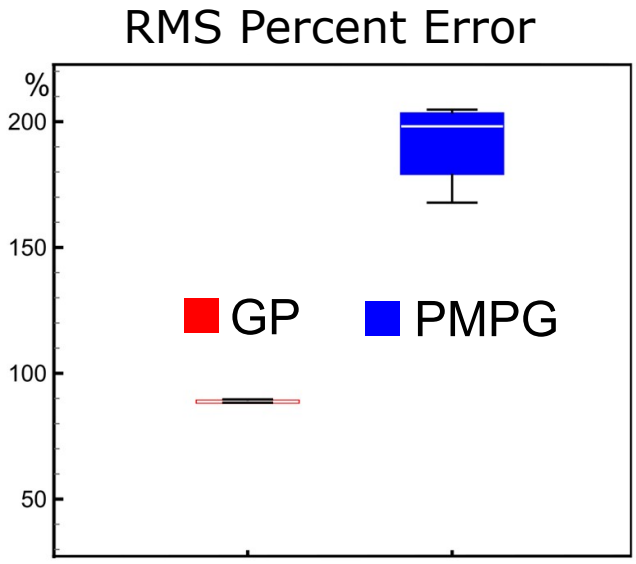

Figure 5.4: Box and whisker plot of the root-mean square of the percent error along $h \in \{0.4, 6\}$ for the GP and PMPG model.

5.2 Leading-edge stagnation angle

The leading-edge stagnation point on the cylinder was compared across the models, which can be seen in figure 5.5. For small $h < 1$, all models under-predict the location of the stagnation point. The leading-edge stagnation point lies between the GP and PMPG model location for most h values, which is indicative of the variational approaches' suitableness in modeling the leading-edge of a cylinder in ground effect. Given that the leading-edge stagnation point is somewhat captured by these auxiliary conditions, it is reasonable to assume that the leading-edge velocity profile is adequately modeled by these models.

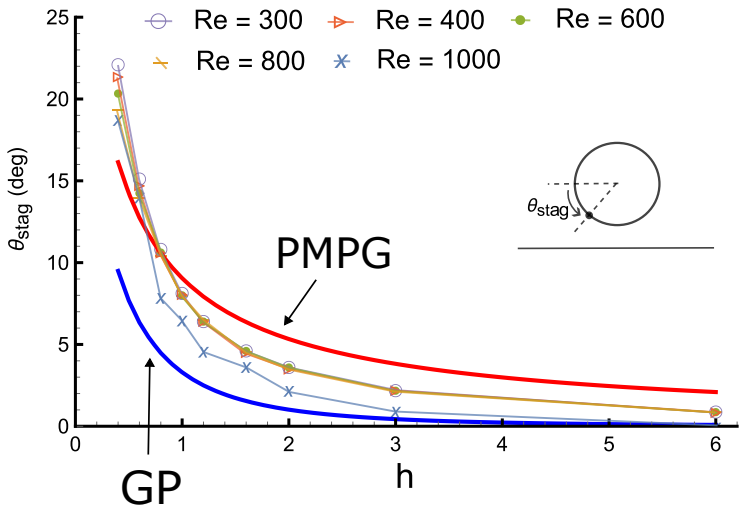

Figure 5.5: Leading-edge stagnation angles from the CFD simulations [1], GP, and PMPG model for $h \in \{0.4, 6\}$.

5.3 Post-processed model

The potential flow model does not include any information about the wake structure behind the cylinder. Given the results in figure 5.5, the leading-edge flow field is assumed to be adequately approximated by the potential flow model. This section explores an approximation of the trailing-edge pressure that captures the wake dynamics in an attempt to improve the original models. This model will be referred to as the **post-processed** model. Since the quantity of interest in this model is the lift coefficient, the pressure profile along the contour is of most importance. The pressure coefficient along the contour is now represented as

$$\text{Pressure} = \begin{cases} \text{Potential Flow Solution} & \text{Leading} - \text{Edge Region} \\ \text{Approximation Function} & \text{Trailing} - \text{Edge Region} \end{cases}. \tag{5.2}$$

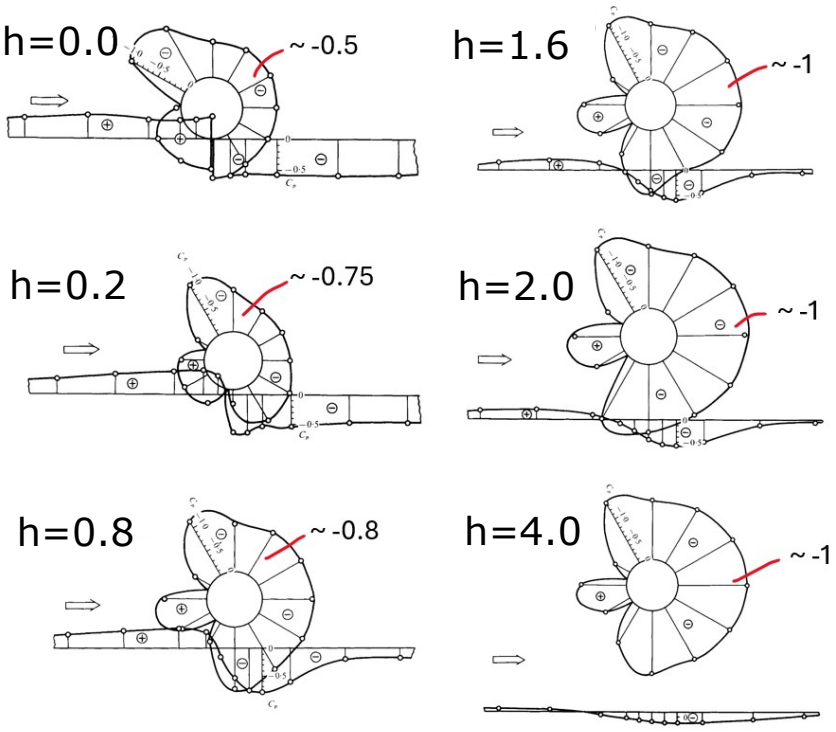

Figure 5.6: Experimental pressure coefficient values around the boundaries at h = 0, 0.2, 0.8, 1.6, 2, & 4 from [2]. The trailing-edge pressure approximation values are shown.

The trailing-edge pressure along the contour is approximated by prior experimental data [2] and the extent of the trailing-edge region is determined by the data given in figure 1.4.

The trailing-edge pressure was estimated based on an experiment conducted by Bearman & Zdravkovich [2], where the pressure coefficient along the contour of a cylinder near a **non-moving** ground was measured and plotted for h values of 0.0, 0.2, 0.8, 1.6, 2.0, and 4.0. This data set was chosen because of the scarcity of available pressure data for a cylinder near a moving ground. Figure 5.6 shows the results by Bearman & Zdravkovich [2], including the estimates used to guide the approximation of the trailing-edge pressure. From their pressure coefficient data, the trailing-edge pressure coefficient for this work was set to $C_p = -1$. Although the pressure coefficient data in [2] deviates from this value from $h \in \{0.4, 1\}$, $C_P \approx -1$ is taken to be a reasonable approximation.

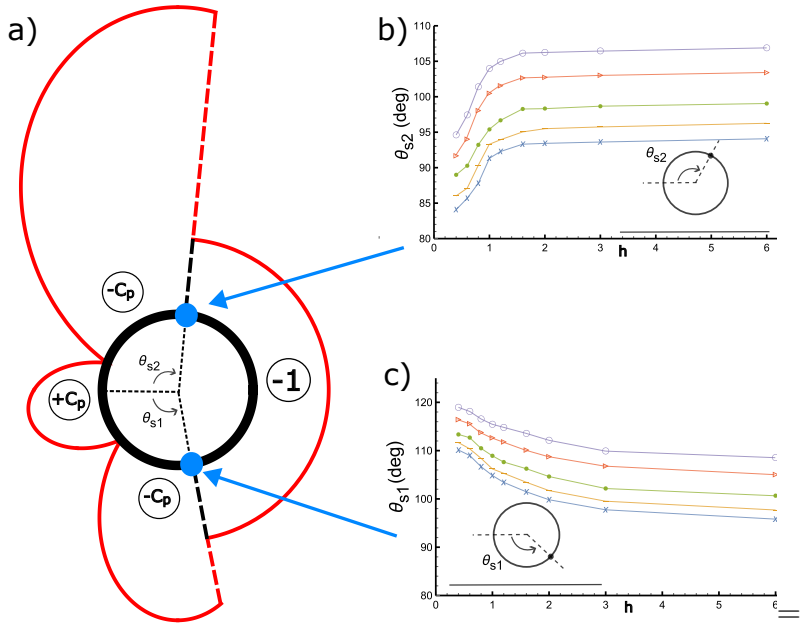

Figure 5.7: Panel *a)* shows a representation of the pressure coefficient distribution around the cylinder at $h = 1$, $Re = 1000$ with a constant pressure in the trailing-edge. The region that constitutes the trailing edge is determined by the flow separation data, seen in panels *b)* and *c)*, from the CFD simulations [1].

The resulting lift coefficient was determined by calculating the leading and trailing edge C_L individually by using the flow separation angles (figure 1.4) to dictate the angle span of each flow regime (potential flow or $C_P = -1$). A representation of the pressure profile around the contour at $h = 1$ and $Re = 1000$ with this methodology is shown in figure 5.7. The separation angles are used as a gross simplification of the wake dynamics, providing the potential model with information that is attempting to improve the physical accuracy of the results.

Baikov & Petrov [34] try to improve the reduced-order model by extending the cylinder's body to include the stagnant zone due to the wake. This approach necessitates adjusting the conformal mapping in order to achieve the new shape of the bluff body, which requires numerical approximations that are computationally heavy and complicated to implement. The authors do not include any information about the results of this approach, making it

difficult to compare results with. For these reasons, this extension was not considered in this work.

Figure 5.8 and 5.9 show the resulting lift coefficients and error compared to the CFD results [1], respectively. The percent error over the h domain was 117.6% and 63.4% for Gold'shtik and PMPG methods, respectively. Notice, this approach shifts the best accuracy from GP to PMPG.

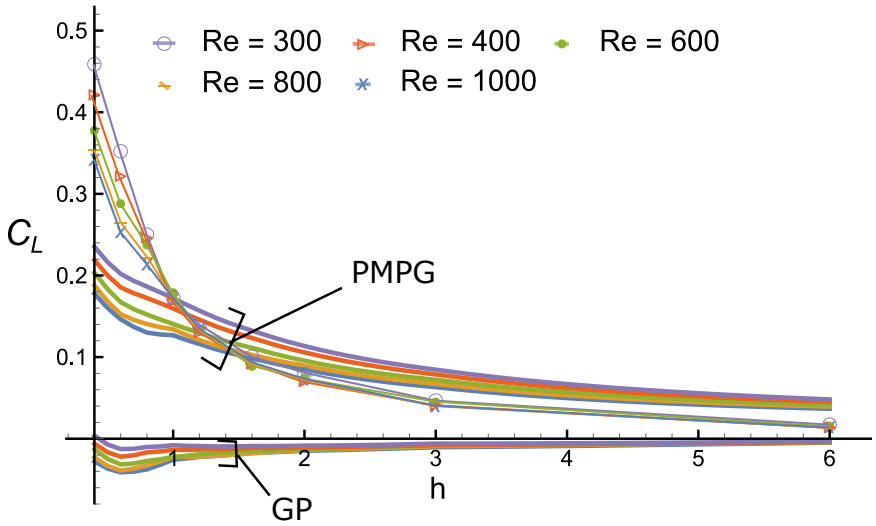

Figure 5.8: Lift coefficient values for GP and PMPG using the post-processed reduced-order model compared with the CFD simulations [1] data.

It is helpful to characterize how the inclusion of the wake structure changes the lift coefficient of a full potential flow model. Figure 5.10 represents the shift in the lift coefficient from the full flow to the post-processed model. By using a constant value of the trailing-edge pressure coefficient, the overall lift coefficient is reduced. This change is not surprising given that stall (induced drag on the body) in an airfoil results in a loss of lift.

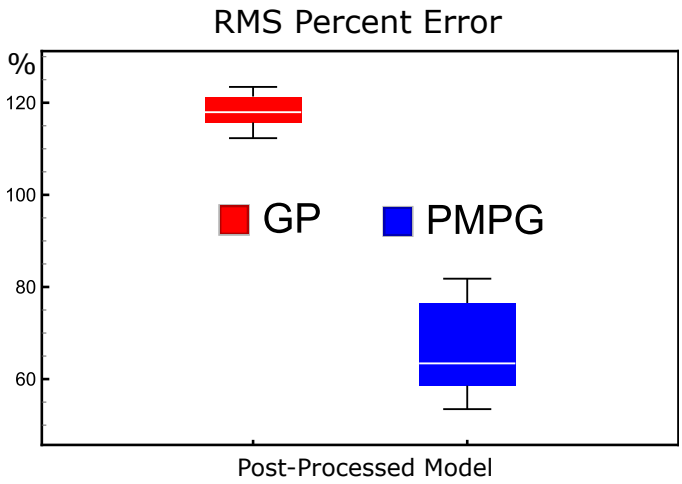

Figure 5.9: Box and whisker plot of the root-mean-square of the percent error along $h \in \{0.4, 6\}$ for the GP and PMPG post-processed model.

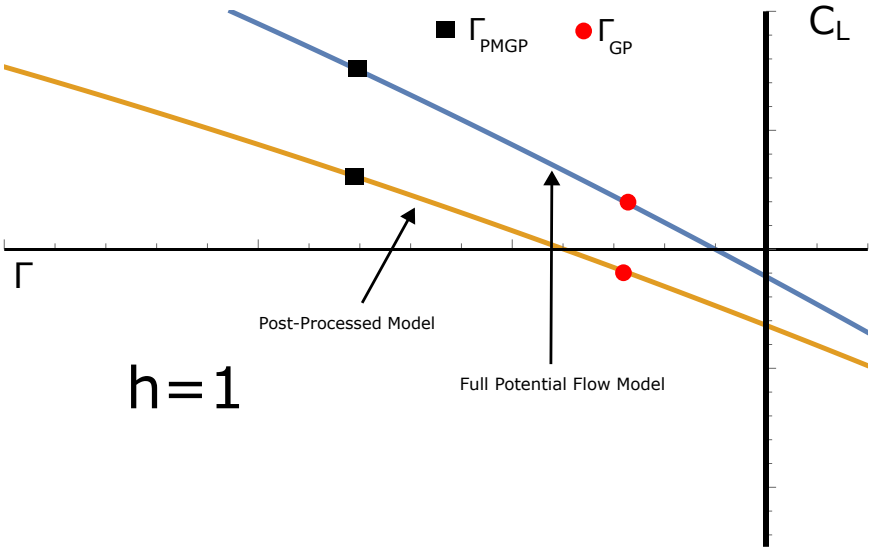

Figure 5.10: The lift coefficient as a function of the circulation for the full potential flow model and the post-processed model.

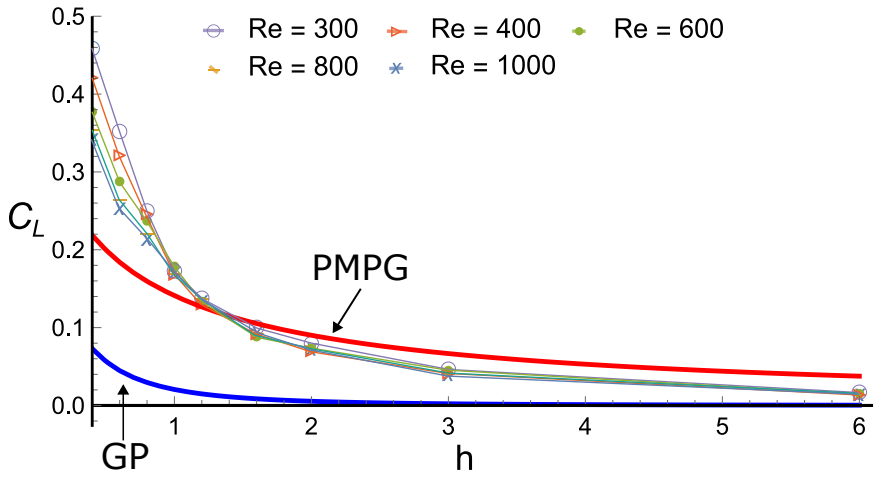

Figure 5.11: Lift coefficient values for GP and PMPG using the semi-processed reduced-order model compared to the CFD simulations data [1].

5.4 Case study: the semi-processed model

Although the inclusion of the wake structure based on separation angles seems to improve the lift coefficient prediction for PMPG, this approach requires specific information about the flow separation from CFD or experiments. Another approximation approach is to simply assume the separation points to be at the top and bottom dead center of the cylinder. Since the separation points are near these points experimentally and computationally anyhow (see figure 1.4), this approximation could yield helpful results without having to have any flow-specific details (i.e., the separation angle data). This model will be referred to as the **semi-processed** model. Since the pressure profile is vertically symmetric (i.e., the leading- and trailing-edge pressure distributions are identical), the corresponding lift coefficients are calculated by dividing the full potential flow lift coefficient by two. The calculated lift coefficient for the semi-processed model can be seen in figure 5.11. The percent error, as seen in figure 5.12, over the h domain was 94.3% and 57.2% for the GP and PMPG methods, respectively.

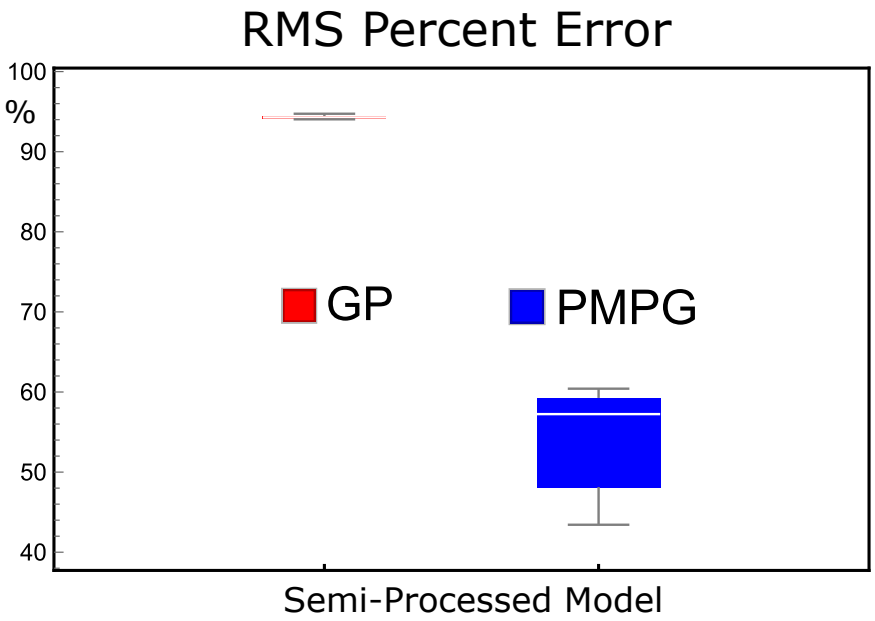

Figure 5.12: Box and whisker plot of the root-mean-square of the percent error along $h \in \{0.4, 6\}$ for the GP and PMPG semi-processed model.

The semi-Gol'dshtik's approach continues to under-predict the lift coefficient, increasing the percent error. However, the semi-PMPG approach captures the correct magnitude of the lift coefficient for $h > 1$, decreasing the percent error relative to the CFD results [1].

A summary of the different approaches for the reduced-order model is shown in figure 5.13. The semi-processed model with PMPG produces the best results for calculating the lift coefficient of a cylinder in ground effect. For both methods that take into account the wake structure, the PMPG outperforms GP by over 35%.

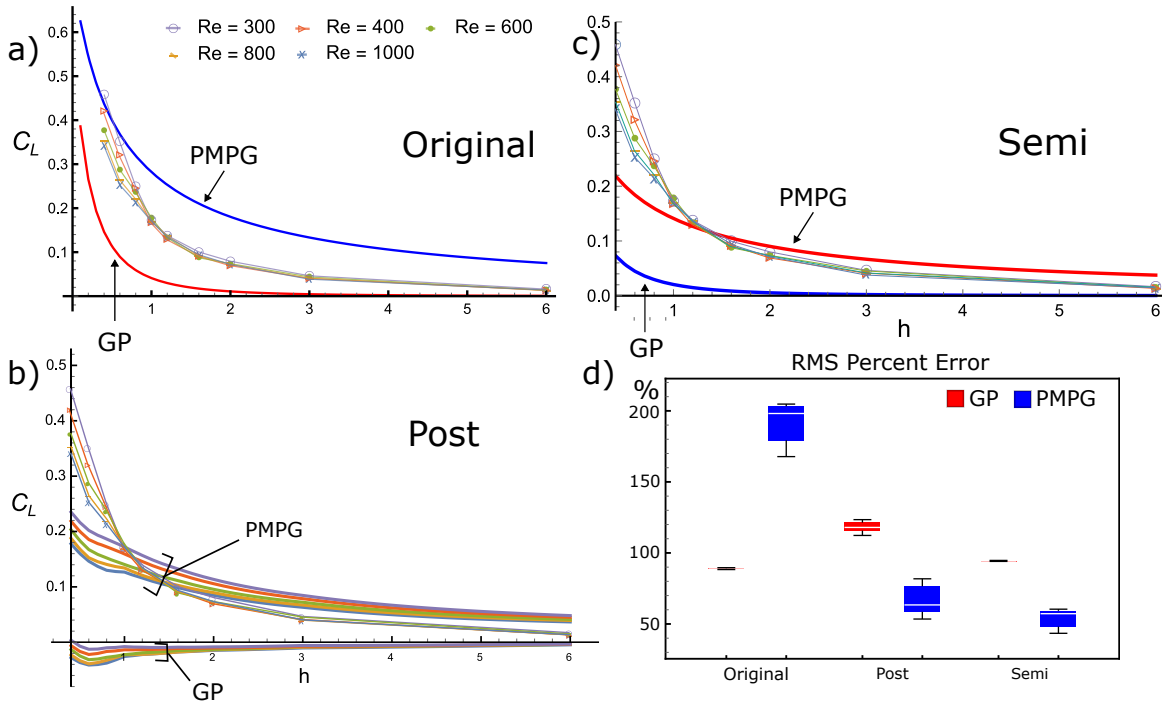

Figure 5.13: Summary of lift coefficient calculations with *(a)* original, *(b)* post-processed, and *(c)* semi-processed reduced-order models using both GP and PMPG auxiliary conditions, and *(d)* the root-mean square errors for each approach.

Chapter 6

Discussion

The general potential flow solution for a cylinder in ground effect with a moving ground was solved previously for an arbitrary choice of cylinder circulation, Γ [19]. However, it is difficult to investigate its utility without an auxiliary condition to determine Γ. Two proposed auxiliary conditions were explored through comparison with a CFD simulation [1]. The accuracy of these models was based on the percent error and empirical overlap between the reduced-order models and the simulation, as well as the theoretical rigor behind the auxiliary condition.

This discussion will consist of 1) investigating the value of a potential flow model for a cylinder in ground effect, and 2) discussing the insight this reduced-ordered model gives into the physics of a cylinder in ground effect. Each section will be decomposed into mini-discussions on Gol'dshtik and PMPG individually.

6.1 Value of potential flow theory for a cylinder in ground effect

Considering the whole flow field as potential flow is not expected to be a very good approximation in this application. When the flow separates from the cylinder, there is a turbulent wake, causing the flow to deviate significantly from the potential flow approximations. It

is somewhat surprising that the potential flow model gets the trend of C_L with h correct for both auxiliary conditions. This result is indicative of the influence of the gap-to-radius ratio, h, to the system's pressure dynamics. The potential flow framework seems to capture significant features of a cylinder in ground effect that convey the overall trend of the lift coefficient. This is remarkable, considering that originally no information about the wake structure is provided to the model.

Although it is helpful to discuss the trends of GP and PMPG assuming the entirety of the flow is potential flow, the use of the model in this form misrepresents the true flow. The predictions made by this approach provide the dynamics of a system where viscosity is neglected (i.e., solving the Euler equation). Any offset between prediction and experiment could be due to the introduction of viscosity in the physical system. If this statement is true, then depending on the variational approach used, there is a way to quantify the lift force induced by the wake structure (which is only introduced with viscosity) in the flow. If GP provides the correct potential flow solution, then the induced wake structure is what is providing the cylinder with the extra positive lift that is computed in experiments and simulations. Here, the wake structure is a lift-generating mechanism. However, if the PMPG method is the correct auxiliary condition for the potential flow solution, then the induced wake structure provides a negative lift to compensate for the over-prediction given by PMPG. The wake structure is a suction-generating mechanism in this case. It is expected that the wake structure is a suction-generating mechanism in this case when considering the effect of lag in airfoils [35]. This related situation provides support for the principle of minimum pressure gradient as providing an accurate auxiliary condition in this system.

Although the potential model does not account for flow separation, it is a helpful approximation for the leading-edge flow. For large Reynolds number ($Re >> 1$), it is assumed that 1) the flow in the trailing-edge region does not largely affect the flow in the leading-

edge region, and 2) the flow is an ideal fluid in the leading-edge region. One method to check the effectiveness of the potential flow model for the leading-edge is by calculating the leading-edge stagnation point given by both auxiliary conditions. Figure 5.5c shows the stagnation point given by the CFD simulations [1], Gol'dshikt's postulate, and PMPG. Although neither model overlaps perfectly with the CFD results, the stagnation angle errors are within 4 degrees. Given the proximity of the models to the CFD results, the leading-edge can be said to be adequately modeled by the potential flow model. Given the leading-edge flow solution, the pressure distribution could be calculated to find the resultant lift in the leading-edge region. With the trailing-edge pressure distribution already determined by previous experiments [2], the lift in the trailing-edge region can be estimated. Adding these two pressure distributions together should result in a prediction of the overall lift experienced by a cylinder in proximity to a moving ground. Additionally, an approximation of this method was studied which assumed the flow separation to be at the poles of the cylinder. These procedures were able to sift through the proposed auxiliary conditions to find the variational principle that provides the most accurate potential flow approximation. Given the resulting lift force, PMPG seems to produce the best auxiliary condition. In the following section both Gol'dshtik and the PMPG method will be examined individually as to their success or lack of success in modeling the leading-edge potential flow model.

6.1.1 Gol'shtik's postulate as auxiliary condition

Including experimentally supported trailing-edge dynamics with the leading-edge potential flow model using Gol'dshtik's auxiliary condition resulted in negative lift for the cylinder at all height-to-radius values. The prediction of suction is physically incorrect and provides support for Gol'dshtik's postulate being an inadequate auxiliary condition. The conclusion is that this model does not accurately capture the leading-edge dynamics of a cylinder moving

near a ground. There are multiple reasons inaccuracy this might be the case.

First, the potential flow model formulation and GP are immediately in conflict regarding flow separation. Gol'dshtik asserts the maximum velocity in the flow is the smallest it can be in order to reduce the magnitude of the negative pressure. The reasoning is that separation can occur where the negative pressure is the greatest. The flow 'selects' the velocity field that reduces the likelihood of separation. Continuing with this reasoning, the separation points will be in the places where the flow has the largest velocity. The potential flow formulation is at odds with this assertion. In the potential formulation, the maximum velocity on the cylinder will **always** be at the poles of the cylinder. This simply does not align with what is seen in experiments. Figure 1.4 shows that the separation points occur at varying angles. This makes GP irreconcilable with both the potential model and CFD results [1]. With one model claiming the location of separation will always be at the poles and then trying to add that to a computationally supported dataset that clearly shows the separation points occurring elsewhere in order to create an accurate representation of the pressure distribution is not physically consistent. Choosing to minimize the maximum velocity on the contour does not seem to be the best auxiliary condition given that the flow system that is minimized is a purely ideal fluid with no indication of separation, something the auxiliary condition inherently assumes occurs in the flow. Although the stagnation point prediction does not indicate that Gol'dshtik's model is a bad approximation, it is clear that this auxiliary condition does an inadequate job at representing the potential flow in the leading-edge when considering the pressure-distribution.

Second, Gol'dshtik's postulate is an auxiliary condition for flows with separation. It is not generalizable to flows without separation. Similar to the first reason, potential flow theory does not account for separation. Even if Gol'dshtik's postulate could produce a physical result, it could prove fruitless in flows that do not experience separation. The postulate

would have to be a specific application of a more general statement for fluids. The lack of generality does not exclude the postulate from being useful, but it gives less support for wanting to use this postulate.

Thirdly, Gol'dshtik's postulate only considers the velocity on the contour. Although separation occurs on the contour, a large portion of the flow system is disregarded by this approach. By limiting the auxiliary condition purely to what is happening to the flow on the boundary, Gol'dshtik is inadvertently claiming that the flow dynamics outside the contour have no **direct** effect on the overall circulation of the system. Not including the surrounding flow in the auxiliary condition may have contributed to Gol'dshtik's unsuccess.

It seems that extending Gol'dshtik's postulate to other fluid problems does not work. Fortunately, the PMPG model fares much better.

6.1.2 The principle of minimum pressure gradient as auxiliary condition

The principle of minimum pressure gradient predicts lift coefficient values similar to the CFD simulations [1] for $h \in \{1, 6\}$ when the experimentally supported trailing-edge pressure distribution is included. For $h < 1$, the model under-predicts the lift on the cylinder, something which is further addressed in section 6.2. This trend is also seen in approximating the separation points to be at the poles. The latter approximation does not require information from experiments or CFD simulations [1] about the separation points and yields better results than GP in calculating the lift coefficient. This accuracy is most likely due to the fact that the separation points are near the poles of the cylinder for $h > 1$. Regardless of which modified model is used, for $h \in \{1, 6\}$ PMPG seems to provide the correct auxiliary condition to capture the leading-edge flow system of flow past a cylinder in proximity to a

moving ground. Again, for $h > 6$ the PMPG seems to approach zero at an exponentially slower rate than both the CFD simulations and GP method. This may be due to an artifact in the computation or the variational approach itself, and should be further investigated.

Although the trailing-edge pressure distribution is a rough approximation in this work, for the regions where the Bearman & Zdravkovich [2] data is most clear (i.e. $h > 1$), the PMPG solution deviates only slightly from the CFD simulations [1]. For smaller h values, the approximation of the trailing-edge pressure distribution needs to be adjusted and understood better. However, the strong overlap between CFD and the PMPG model provides support that PMPG is an acceptable auxiliary condition and that a potential flow model can adequately describe flow dynamics at the leading-edge. There could be multiple reasons for this acceptability being the case.

First, Gauss' principle is a general statement that reduces to the principle of minimum pressure gradient for incompressible flow. It can be shown that Gauss' principle is equivalent to D'Alembert's principle [33], the form of analysis widely used in mechanics. The theoretical backbone of Gauss' principle provides better support for its application to a cylinder in ground effect over Gol'dshtik's postulate. The leading-edge potential flow model was probably best captured by PMPG because the flow is truly minimizing the pressure gradient in that region.

Second, PMPG takes into account the entire flow field. Since the principle is concerned with the overall minimization of the pressure gradient, the resulting circulation value is dictated by what occurs on the contour of the cylinder as well as at infinity. Unlike GP, which considers infinity only in an indirect manner, PMPG explicitly considers the flow everywhere. This may have contributed to its success because it does not neglect all the (spatial) factors contributing to the final flow field.

Thirdly, the pressure gradient is a much more significant quantity in the flow field than the magnitude of the pressure. A reason separation can occur is because of the pressure **change**. Minimizing the pressure gradient is nature's most direct method of resisting separation, rather than simply minimizing the magnitude of the pressure. The principle of minimum pressure gradient gets to the core of separation as opposed to Gol'dshtik's postulate.

The extension of Gauss' principle to flows is new [32] and merits more investigation. Although Gauss' principle is equivalent to Lagrangian mechanics, it is an old and 'unused' principle that requires thorough vetting. It is the hope that this work provides support for Gauss' principle being a relevant and insightful tool in the area of fluid mechanics. Maybe all incompressible flows are truly minimizing the pressure gradient in all space and time.

6.1.3 The best model

For the models considered, the **semi-processed** model using PMPG seems to capture the CFD results best when considering the lift coefficient calculations. This approach requires no knowledge of the flow separation and provides a reduced-order model of the lift coefficient for a cylinder in ground effect for $h \in \{1, 6\}$.

6.2 Physical insight from PMPG

Given that PMPG accurately calculates the leading-edge lift for h values greater than one, it is safe to assume that the potential model is an adequate model for the leading-edge. The discrepancy between the model and the CFD results [1] for $h \in \{0.4, 1\}$ can be attributed to the approximation taken for the trailing-edge pressure distribution. Using the plots by Bearman & Zdravkovich [2], for small values of h the position of the flow separation and

trailing-edge pressure coefficient dramatically change. The experiments used for the trailing-edge pressure were conducted on a cylinder near a **non-moving** ground, so the results given by them at smaller h values are not necessarily reliable for this situation of a moving ground. The lack of experimental data in this regime makes it difficult to assess the validity of assuming the leading-edge is properly modeled by potential flow theory. However, if the Bearman & Zdravkovich [2] data give an accurate indication of flow behavior, regardless of the moving ground assumption, it is clear that the trailing-edge C_P at small h is not accurately given by the approximations being made here for the trailing-edge C_P at larger h.

For a cylinder in ground effect, the leading-edge flow, when approximated as an ideal flow, is able to adequately estimate the magnitude and trend of the lift coefficient for gap-to-radius ratios greater than one. It is remarkable that when applying a potential flow model to the entire domain of a cylinder in ground effect (e.g., excluding wake effects) the overall trend of the lift coefficient is captured. The geometric parameter, h, clearly plays a significant role in the form and structure of the lift coefficient for a cylinder in ground effect. For small h the leading-edge region may still be represented, but the contribution from the wake may begin to dominate, and/or just deviate significantly from $C_p = -1$. The significance of the parameter, h, requires much more study. As provided in the introduction 1, there is still great misunderstanding of the wake dynamics at small h values. The ground introduces enough asymmetry in the wake structure that the approximations used in this work are no longer adequate at h values of less than approximately 1.

6.3 Future work

There are improvements and extensions to this work that could be implemented for the analytical formulation of bodies in ground effect. Having an adequate experimental understanding of the pressure-distribution along the contour would help dramatically, especially in understanding the large discrepancy in calculated lift at small h values. This information would aid in determining the validity of the potential flow formulation of the leading-edge. Acquiring experimental data of this information at multiple Reynolds numbers and height-to-radius ratio is still required to gain understanding of the wake structure at small h values. It would also be helpful to use the CFD simulations [1] angle separation data and find the best-fit model as a function of Reynolds numbers and height-to-radius ratio. In this way the analytical model could be used to calculate the lift coefficients for Reynolds numbers not explicitly calculated in the CFD paper [1]. Finding a best-fit model of Bearman's & Zdravkovich's [2] trailing-edge pressure distribution would be helpful; however, since their system had a **non-moving** ground it would be best to have experimental data of the trailing-edge pressure for a system that has a **moving** ground.

Another improvement for the potential flow model is that rather than calculating the flow around a cylinder, one could model the flow around the bluff body that consists of the cylinder and the stagnation zone created by the wake, as done by Petrov [18] using GP. This approach will allow for a circulation calculation that takes into the account the structure of the wake, which could allow for a more accurate circulation value for the potential flow model. An alternative to this approach is to use free streamline theory to capture the extended body. Although this approach would capture the 'shape' better, these extensions are typically not analytical and may require detailed information about the wake structure.

In Baddoo's paper [19], he provides exact solutions for different types of flows for varying

types of airfoils over ground. In addition to modeling uniform and straining flow, the paper includes a method to implement point vortices in the flow. This addition could be helpful in modeling the vortex shedding of a cylinder in a free stream. Besides a cylinder, his paper [19] includes airfoils such as a flat plate, curved plate, ellipses, and flapping wings for any of these shapes. Investigating the versatility of the potential model for these different flow systems could be extremely helpful. For example, a flat plate at small angles of attack does not have separation, which makes it a suitable candidate for a potential flow model for the **entire** spatial domain. Also, studying the flow around an ellipse near ground would aid in the discussion of sea animal locomotion (think sting ray) near seabeds. The ability to create potential flow models of flapping wings also begs the question of its utility in representing time-dependent hydrodynamics. The role of time dependence is still to be investigated and having an auxiliary condition that gives a closed-form solution would be a great tool in studying these systems.

The final area that is worthy of exploration is connecting Gauss' principle with Hamilton's principle. Given that Gauss' and D'Alembert's principles are equivalent [33], rewriting Gauss' principle in terms of Hamilton's principle would be revolutionary in the area of fluids. Hamilton's principle is the bread and butter of solid mechanics, and being able to apply it to fluids would allow for studying fluid-structure interaction problems in a new light. Verifying Gauss' principle would also provide new fundamental information about incompressible flows that extend far beyond potential flow modeling, by answering the age old question of how lift is generated in the first place [32]. The new variational approach for fluids carries with it a lot more questions than have been answered; this present work supports the utility of Gauss' principle in modeling the pressure-profile of flow past a cylinder near a moving ground.

Chapter 7

Conclusion

It is helpful to recap the approximations taken in this study to demonstrate the robustness of this model. For the leading-edge region, the assumptions are:

1. the flow is incompressible,
2. the flow is inviscid,
3. the flow is irrotational,
4. the flow is steady,
5. there is no slip on the contour of the cylinder and the ground,
6. the ground is moving at the same speed as the background flow,
7. the 3D flow system can be studied as a 2D slice,
8. the flow can be modeled by potential flow;

and for the trailing-edge region the assumptions are

1. the pressure distribution along the trailing-edge contour is the constant value of the dynamic pressure, and
2. the pressure values are determined from an experiment considering a cylinder near a **non-moving** ground,

or

1. the pressure distribution along the trailing-edge contour is the constant value of the dynamic pressure, and
2. the flow separation is chosen to occur at the top and bottom dead center of the cylinder.

With these assumptions, the lift coefficient values were adequately captured for the regime $h \in \{1, 6\}$. The magnitude and trend in C_L as calculated by PMPG is similar to the CFD simulation results [1] for a cylinder in ground effect when applying an asymmetry between the leading and trailing edge flow dynamics. The model is robust under all the approximations, which highlights how significant the geometry alone is in the overall dynamics of the problem.

Constructing an improved analytical model that calculates the lift of a cylinder in a moving flow in proximity to a flat surface was the aim of this work. For the leading-edge region, a potential flow solution was used to capture the pressure profile in this region. The trailing-edge pressure distribution was determined by prior experiments conducted on a similar flow system. However, the flow separation points were located at the poles of the cylinder. This approach accurately calculated the lift on the cylinder at height-to-radius ratios above one. The model is robust even under the many approximations and gives clear insight into the interplay between the height-to-radius parameter and the introduction of an asymmetric wake in the flow field due to the ground's presence.

There is now an improved analytical formulation for the lift on a cylinder in ground effect, something that has not been thoroughly investigated before. This analytical formulation 1) gives support for PMPG method being applied for incompressible flows, and 2) the potential flow model is an adequate approximation of the leading-edge flow for this problem. May this work contribute to a comprehensive analytical formulation for a cylinder in ground effect and further the exploration of PMPG to other fluid dynamic problems.

Bibliography

[1] Hongyi Jiang, Xiaoying Ju, Zhen Guo, and Lizhong Wang. Turbulent wake characteristics for a circular cylinder in proximity to a moving wall. *Journal of Fluid Mechanics*, 983:A18, March 2024.

[2] P. W. Bearman and M. M. Zdravkovich. Flow around a circular cylinder near a plane boundary. *Journal of Fluid Mechanics*, 89(1):33–47, November 1978.

[3] C H K Williamson. Vortex Dynamics in the Cylinder Wake.

[4] J. H. Gerrard. Flow around circular cylinders; volume 1. fundamentals. by m. m. zdravkovich. oxford science publications, 1997. 672 pp. £120. *Journal of Fluid Mechanics*, 350:375–378, 1997.

[5] M.M. Zdravkovich. Forces on a circular cylinder near a plane wall. *Applied Ocean Research*, 7(4):197–201, October 1985.

[6] C. Lei, L. Cheng, and K. Kavanagh. Re-examination of the effect of a plane boundary on force and vortex shedding of a circular cylinder. *Journal of Wind Engineering and Industrial Aerodynamics*, 80(3):263–286, 1999.

[7] S.J. PRICE, D. SUMNER, J.G. SMITH, K. LEONG, and M.P. PAÏDOUSSIS. Flow visualization around a circular cylinder near to a plane wall. *Journal of Fluids and Structures*, 16(2):175–191, 2002.

[8] Muk Ong, Torbjørn Utnes, Lars Erik Holmedal, Dag Myrhaug, and Bjornar Pettersen. Numerical simulation of flow around a circular cylinder close to a flat seabed at high reynolds numbers using a k– model. *Coastal Engineering*, 57:931–947, 10 2010.

[9] Ming Zhao and Liang Cheng. Two-dimensional numerical study of vortex shedding regimes of oscillatory flow past two circular cylinders in side-by-side and tandem arrangements at low reynolds numbers. *Journal of Fluid Mechanics*, 751:1–37, 2014.

[10] Weilin Chen, Md. Mahbub Alam, Yuzhu Li, and Chunning Ji. Two-degree-of-freedom flow-induced vibrations of a D-section prism. *Journal of Fluid Mechanics*, 971:A5, September 2023.

[11] Jianghua Li, Bofu Wang, Xiang Qiu, Jianzhao Wu, Quan Zhou, Shixiao Fu, and Yulu Liu. Three-dimensional vortex dynamics and transitional flow induced by a circular cylinder placed near a plane wall with small gap ratios. *Journal of Fluid Mechanics*, 953:A2, December 2022.

[12] Takafumi Nishino, Graham T. Roberts, and Xin Zhang. Vortex shedding from a circular cylinder near a moving ground. *Physics of Fluids*, 19(2):025103, February 2007.

[13] Wei-Xi Huang and Hyung Jin Sung. Vortex shedding from a circular cylinder near a moving wall. *Journal of Fluids and Structures*, 23(7):1064–1076, 2007.

[14] A. Rao, M.C. Thompson, T. Leweke, and K. Hourigan. The flow past a circular cylinder translating at different heights above a wall. *Journal of Fluids and Structures*, 41:9–21, 2013. Special issue on Bluff Body Flows (Blubof2011).

[15] H.S. Yoon, J.B. Lee, J.H. Seo, and H.S. Park. Characteristics for flow and heat transfer around a circular cylinder near a moving wall in wide range of low reynolds number. *International Journal of Heat and Mass Transfer*, 53(23):5111–5120, 2010.

[16] Takafumi Nishino. DYNAMICS AND STABILITY OF FLOW PAST A CIRCULAR CYLINDER IN GROUND EFFECT.

[17] Alex Mendonça Bimbato, Luiz Antonio Alcântara Pereira, and Miguel Hiroo Hirata. Simulation of viscous flow around a circular cylinder near a moving ground. *Journal of the Brazilian Society of Mechanical Sciences and Engineering*, 31(3):243–252, September 2009.

[18] A. G. Petrov and D. V. Maklakov. On Determining Circulation for a Flow around a Cylinder near a Plane Wall. *Fluid Dynamics*, 57(7):900–910, December 2022.

[19] Peter J. Baddoo, Melike Kurt, Lorna J. Ayton, and Keith W. Moored. Exact solutions for ground effect. *Journal of Fluid Mechanics*, 891:R2, May 2020.

[20] Koichi Oshima. Some remarks on the kutta condition. In *Advances in Fluid Dynamics*, pages 218–227, New York, NY, 1989. Springer New York.

[21] P. G. Daniels. ON THE UNSTEADY KUTTA CONDITION. *The Quarterly Journal of Mechanics and Applied Mathematics*, 31(1):49–75, 1978.

[22] D G Crighton. The Kutta Condition in Unsteady Flow.

[23] J. P. Giesing. Vorticity and Kutta Condition for Unsteady Multienergy Flows. *Journal of Applied Mechanics*, 36(3):608–613, September 1969.

[24] Massimo Gennaretti and Riccardo Giansante. Kutta–Joukowski Theorem for Unsteady Linear Aerodynamics. *AIAA Journal*, 60(10):5779–5790, October 2022.

[25] M. A. Gol'dshtik and V. M. Khanin. Interaction of a cylinder with a free surface and a jet. *Fluid Dynamics*, 12(5):683–690, 1978.

[26] Cody Gonzalez and Haithem E. Taha. A variational theory of lift. *Journal of Fluid Mechanics*, 941:A58, June 2022.

[27] Darren Crowdy. Schwarz–Christoffel mappings to unbounded multiply connected polygonal regions. *Mathematical Proceedings of the Cambridge Philosophical Society*, 142(2):319–339, March 2007.

[28] G. K. Batchelor. *An Introduction to Fluid Dynamics*. Cambridge Mathematical Library. Cambridge University Press, 2000.

[29] Sia Nemat-Nasser and Y. C. Fung. Variational methods in the mechanics of solids. *Journal of Biomechanical Engineering*, 104(1):76–76, 02 1982.

[30] Castrenze Polizzotto. An energy approach to the boundary element method. part i: Elastic solids. *Computer Methods in Applied Mechanics and Engineering*, 69(2):167–184, 1988.

[31] Q. Yang, L. Stainier, and M. Ortiz. A variational formulation of the coupled thermo-mechanical boundary-value problem for general dissipative solids. *Journal of the Mechanics and Physics of Solids*, 54(2):401–424, 2006.

[32] Haithem E. Taha and Cody Gonzalez. What Does Nature Minimize In Every Incompressible Flow?, March 2022. arXiv:2112.12261 [physics].

[33] Ekkehard Ramm. Principles of least action and of least constraint. *GAMM-Mitteilungen*, 34(2):164–182, 2011.

[34] N. D. Baikov and A. G. Petrov. On a Flow Around a Cylinder Over Uneven Bottom. *Computational Mathematics and Mathematical Physics*, 63(3):401–412, March 2023.

[35] S. B. Gupta, Rajesh K. Tyagi, Pratiksha, and Ayush Gairola. A review on evolution of airfoils and their characteristics in last three centuries. part-1: Evolution of flights and shapes of wing sections before 1930 and naca series. *AIP Conference Proceedings*, 2597(1):070002, 12 2022.

Appendices

Appendix A

Integral Statements

=

A.1 Integration Scheme

All the integral terms are evaluated in the spatial domain Ω,

$$\begin{aligned} &\int_{\Omega} d\Omega \\ &\int_{\partial\Omega} d(\partial\Omega). \end{aligned} \tag{A.1}$$

As a reminder, the reference frame is the ζ-plane and the physical frame is the z-plane. The area element $d\Omega$ is in the z-plane. However, we want to integrate in ζ coordinates since those are the coordinates we have written our complex velocity and it also gives an easier contour to integrate over. The change of the area element from $dz \to d\zeta$ can be written as $d\Omega = Jd\Omega^{\#}$, where J is the Jacobian. The Jacobian in complex notation can be written as

$$J = |\frac{dz}{d\zeta}|^2 = |g'(\zeta)|^2. \tag{A.2}$$

Thus our change in area elements can be rewritten as

$$d\Omega = \frac{d\Omega^{\#}}{|G|^2}, \tag{A.3}$$

where $\Omega^{\#}$ is in ζ-plane coordinates.

Taking advantage of the fact that the material shape of the annullus transforms into the whole field of a cylinder in ground effect, recall figure 2.2, the area of integration in the material frame is the entire annullus with $r \in \{q, 1\}$ and $\theta \in \{0, 2\pi\}$. Using polar coordinates the area element is $d\Omega^{\#} = rdrd\theta$. Our integrals are then rewritten as

$$\int_{\Omega} d\Omega \to \int_{0}^{2\pi} \int_{q}^{1} \frac{rdrd\theta}{|G(re^{i\theta})|^2} \tag{A.4}$$

Treatment for the contour integrals is similar. Complex analysis is well suited for line integrals, by definition

$$\int_{\partial\Omega} d(\partial\Omega) = \int_{\partial\Omega} dz. \tag{A.5}$$

Differentiating equation 2.5 the following is true

$$\int_{\partial\Omega} dz = \int_{\partial\Omega} \frac{d\zeta}{G} \tag{A.6}$$

The inner circle C_0 of the annullus transforms into the contour of the cylinder in the physical space. Thus, the contour in the ζ-plane is defined as $\partial\Omega^{\#} = qe^{i\theta}$ for $\theta \in \{0, 2\pi\}$. The integral can then be expressed as

$$\int_{\partial\Omega} d(\partial\Omega) \to \int_{0}^{2\pi} \frac{i\, qe^{i\theta}\, d\theta}{G(re^{i\theta})}. \tag{A.7}$$